applied sciences

MDPI

Article

HMT-Controlled Synthesis of Mesoporous NiO Hierarchical Nanostructures and Their Catalytic Role towards the Thermal Decomposition of Ammonium Perchlorate

Songzhong Ye and Xiangfeng Guan *

Organic Optoelectronics Engineering Research Center of Fujian's Universities, Fujian Jiangxia University, Fuzhou 350108, China

* Correspondence: xfguan@fjjxu.edu.cn; Tel.: +86-591-2353-1652

Received: 31 May 2019; Accepted: 25 June 2019; Published: 27 June 2019

Abstract: In this work, mesoporous nickel oxide (NiO) hierarchical nanostructures were synthesized by a facile approach by hydrothermal reaction and subsequent calcination. The phase structure, microstructure, element composition, surface area, and pore size distribution of the as-prepared products were characterized by X-ray diffraction (XRD), scanning electron microscopy (SEM), X-ray photoelectron spectroscopy (XPS), and the Brunauer–Emmett–Teller (BET) technique. The precursor of $Ni_3(NO_3)_2(OH)_4$ nanosheet, $Ni_3(NO_3)_2(OH)_4$ microsphere, and $Ni(HCO_3)_2$ sub-microsphere was obtained by hydrothermal reaction at 160 °C for 4 h when the ratio of Ni^{2+}/HMT (hexamethylenetetramine) was 2:1, 1:2, and 1:3, respectively. After calcination at 400 °C for 2 h, the precursors were completely transformed to mesoporous NiO hierarchical nanosheet, microsphere, and sub-microsphere. When evaluated as additives of the thermal decomposition of ammonium perchlorate (AP), these NiO nanostructures significantly reduce the decomposition temperature of AP, showing obvious catalytic activity. In particular, NiO sub-microsphere have the best catalytic role, which can reduce the high temperature decomposition (HTD) and low temperature decomposition (LTD) temperature by 75.2 and 19.1 °C, respectively. The synthetic approach can easily control the morphology and pore structure of the NiO nanostructures by adjusting the ratio of Ni^{2+}/HMT in the reactants and subsequent calcination, which avoids using expensive templates or surfactant and could be intended to prepare other transition metal oxide.

Keywords: HMT-controlled synthesis; NiO; mesopores; hierarchical nanostructures; catalytic activity

1. Introduction

Mesoporous metal oxide MO (M = Ni, Cu, Zn, etc.) materials have attracted much attention due to their large pore volume, high specific surface area, large number of surface reactive sites, and rich material transport channels [1]. Accordingly, these materials are widely applied in many important fields. Among them, nickel oxide (NiO) is an important semiconductor functional material [2], which is widely used in lithium ion batteries [3], electrocatalysis [4], thermal catalysis [5], gas sensor [6], electrochemistry [7,8], optical sensor [9] and biosensors [10–14] fields. Therefore, the preparation of various mesoporous NiO nanomaterials has become a research hotspot.

Up to date, researchers have tried to synthesize mesoporous NiO materials by various synthetic methods, with an aim to improve the properties of materials by optimizing porous nanostructures. For instance, Liu et al. [15] synthesized porous NiO hierarchical microflowers with improved H_2S gas sensing properties. Zhou et al. [16] prepared hierarchical NiO nanoflakes using polyvinylpyrrolidone as a surfactant, which exhibited enhanced gas sensing properties for CH_4 detection. Ahirwar et al. [17]

developed a sol-gel method to prepare porous NiO nanostructures using Tween-80 as a non-ionic surfactant and demonstrated excellent photocatalysis and sensing properties. Zhang et al. [18] reported NiO hierarchical flower-like nanostructures prepared by the solvothermal method, in which cetyltrimethylammonium bromide was used as a surfactant. Han et al. [19] synthesized hierarchical NiO tremella-like and pinecone-like microspheres by the solvothermal method. The NiO microspheres demonstrated good supercapacitor properties. Cai et al. [20] used α-$Ni(OH)_2$ as a precursor to prepare chrysanthemum-like NiO microspheres which exhibited superior lithium storage properties. Hong et al. [21] prepared porous NiO hierarchical microtubes by a novel template-free method, which exhibited superior electrochemical performance due to their high surface area and pore volume.

Although some progress has been made, most of the reported methods require surfactants or templates, and thus it is difficult to obtain mesoporous NiO hierarchical materials with multi-morphologies and controllable pore structure. Therefore, it is highly desirable to develop a facile approach to mesoporous NiO hierarchical materials with multi-morphologies.

In this paper, we developed a rapid and easy approach to mesoporous NiO hierarchical nanostructures by hydrothermal reaction and subsequent calcination. By adjusting the ratio of Ni^{2+}/HMT (hexamethylenetetramine) in a hydrothermal reaction, the precursors of $Ni_3(NO_3)_2(OH)_4$ nanosheet, $Ni_3(NO_3)_2(OH)_4$ microsphere, and $Ni(HCO_3)_2$ sub-microsphere were prepared, which transformed to mesoporous NiO nanosheets, microspheres, and sub-microspheres by simple calcination. These mesoporous NiO nanostructures can effectively reduce the thermal decomposition temperature of ammonium perchlorate (AP), thereby indicating the potential application as additives for AP thermal decomposition. The approach reported here could be intended to prepare other transition metal oxide.

2. Materials and Methods

2.1. Synthesis of NiO Nanostructures

The precursor was prepared by the hydrothermal method which can transform to NiO by subsequent calcination. In the experiments, nickel chloride hexahydrate puratrem ($Cl_2H_{12}NiO_6$, Sinopharm Chemical Reagent Co., Ltd., Shanghai, China) and HMT ($C_6H_{12}N_4$, Sinopharm Chemical Reagent Co., Ltd., Shanghai, China) were used as raw materials, and deionized water as reaction solvent. The experimental process was as follows: $Cl_2H_{12}NiO_6$ was firstly dissolved in deionized water to get 0.2 M Ni^{2+} solution, and then HMT was added the solution under stirring to obtain the mixed solution. The mixed solution was then transferred to the stainless-steel autoclave at 160 °C for 4 h to obtain the precursor product. Among them, the molar ratios of Ni^{2+}/HMT were 2:1, 1:2, and 1:3 for the synthesis of nickel oxide precursor nanosheets, microspheres, and sub-microspheres, respectively. After being cleaned and dried, the as-prepared precursors were put into a high-temperature furnace and calcined at 400 °C for 2 h at a heating rate of 2 °C/min. Finally, mesoporous NiO hierarchical nanomaterials with multi-morphologies were obtained.

2.2. Sample Characterization

X-ray diffraction (XRD, Rigaku MiniFlex II, Rigaka, Tokyo, Japan) was used to characterize the phase structure of the synthesized precursor and its calcined products, using Cu Kα radiation (λ = 0.15406 nm) as the X-ray source. Scanning electron microscopy (SEM, JEOL JSM-6700-F, JEOL, Tokyo, Japan) was adopted to observe the morphology of the samples. Transmission electron microscopy (TEM, JEM-2010, JEOL, Tokyo, Japan) was used to observe the microstructure and morphology of the samples. X-ray photoelectron spectroscopy (XPS, ESCA-LABM250XI, Waltham, MA, USA) was used to characterize the composition and chemical valence of the NiO sample. The surface area and porosity analyzer (ASAP2460, Micromeritics, Norcross, GA, USA) was used to study the specific surface area and pore size distribution of the samples by the Brunauer-Emmett-Teller (BET) and Barrett–Joyner–Halenda (BJH) models, respectively.

2.3. Catalytic Role Study

The catalytic role of NiO additive was evaluated by comparing the thermal decomposition behavior of AP with and without NiO additives. The experiment was carried on a differential thermal analyzer (DTA, Netzsch Model STA449F3). During the experimental process, 5 mg of mixture of AP (98 wt%) and NiO additive (2 wt%) or pure AP was placed into an open Al_2O_3 crucible and heated in nitrogen atmosphere with a heating rate of 15 °C/min among the temperature range of 30–550 °C.

3. Results and Discussion

3.1. Characteriziaton of Phase Structure and Microstructure

The phase structure and morphology of the as-prepared precursors were characterized by XRD and SEM, respectively, as shown in Figure 1. Figure 1a shows the XRD results of as-prepared precursors. When the ratio of Ni^{2+}/HMT is 2:1 and 1:2, all the diffraction peaks of the precursor can be indexed as $Ni_3(NO_3)_2(OH)_4$ phase by JCPDS (Joint Committee on Powder Diffraction Standards) card (No. 22-0752) [22]. When the ratio of Ni^{2+}/HMT is 1:3, the diffraction peaks of the precursor can be indexed to $Ni(HCO_3)_2$ phase (JCPDS card No. 15-0782) [23]. Figure 1b–d show the SEM images of the as-prepared precursors. It can be seen that when the ratio of Ni^{2+}/HMT is 2:1, the product consists of many nanosheets with an average width of about 1 μm; when the ratio of Ni^{2+}/HMT is 1:2, the product is composed of microspheres with a size of 3–5 μm; when the ratio of Ni^{2+}/HMT is 1:3, the product aggregates 100–200 nm of sub-microspheres. In short, the precursors of $Ni_3(NO_3)_2(OH)_4$ nanosheets, $Ni_3(NO_3)_2(OH)_4$ microspheres, and $Ni(HCO_3)_2$ sub-microspheres are obtained by adjusting the ratio of Ni^{2+}/HMT from 2:1 to 1:2 or 1:3 by our synthesis method.

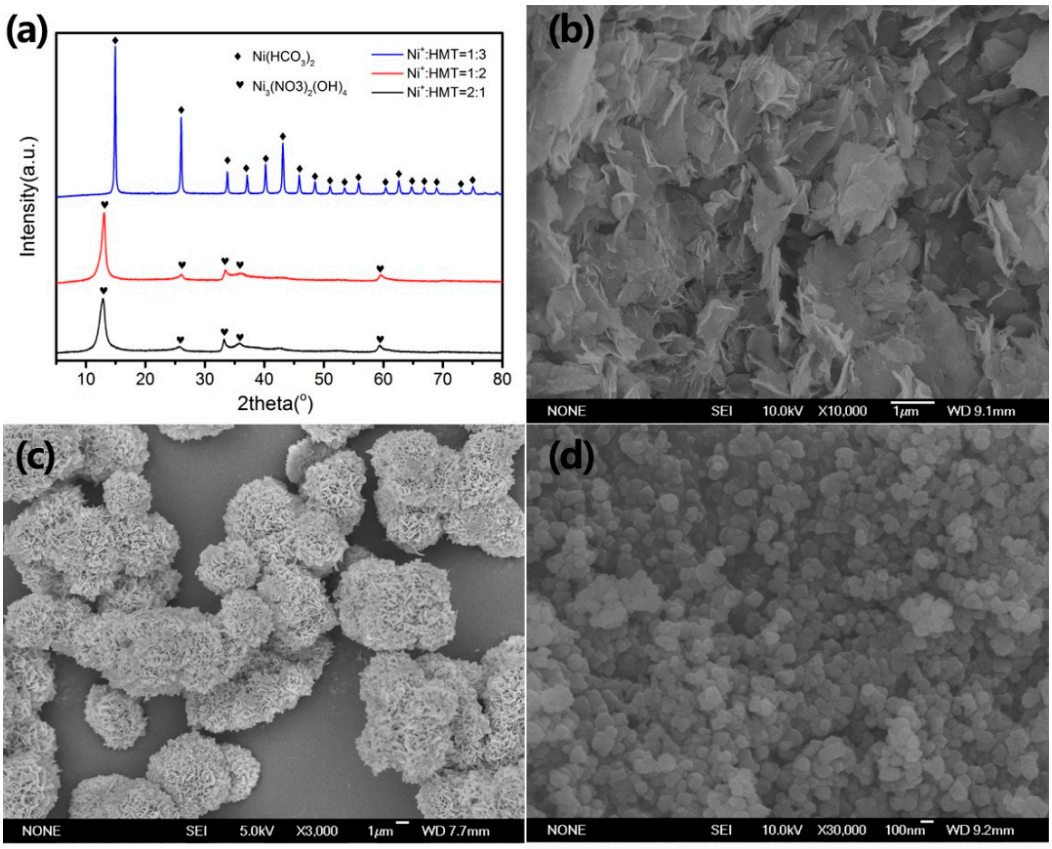

Figure 1. (**a**) XRD (Cu Kα, λ = 0.15406 nm) patterns and SEM (secondary electron imaging mode) images of as-prepared precursor obtained by different ratios of Ni^{2+}/HMT (hexamethylenetetramine): (**b**) 2:1; (**c**) 1:2; and (**d**) 1:3.

The precursors were calcined at 400 °C for 2 h to obtain the NiO samples. Figure 2 shows the XRD and SEM images of the calcined samples. It can be seen from Figure 2a that the calcined products were well indexed to the NiO phase (JCPDS card No. 47-1049) [24], and no impurity phases such as Ni and $Ni(OH)_2$ were found. It indicates that the precursor was transformed into pure NiO phase after calcination. Figure 2b–d show SEM images of as-prepared NiO samples. By comparing the morphology of precursors in Figure 1b–d, it is obvious that the morphologies of NiO samples are basically the same as the overall morphologies of the corresponding precursors, which indicates the good structure stability of the materials during calcination. Therefore, NiO nanosheets, microspheres, and sub-microspheres were successfully prepared by calcining precursors.

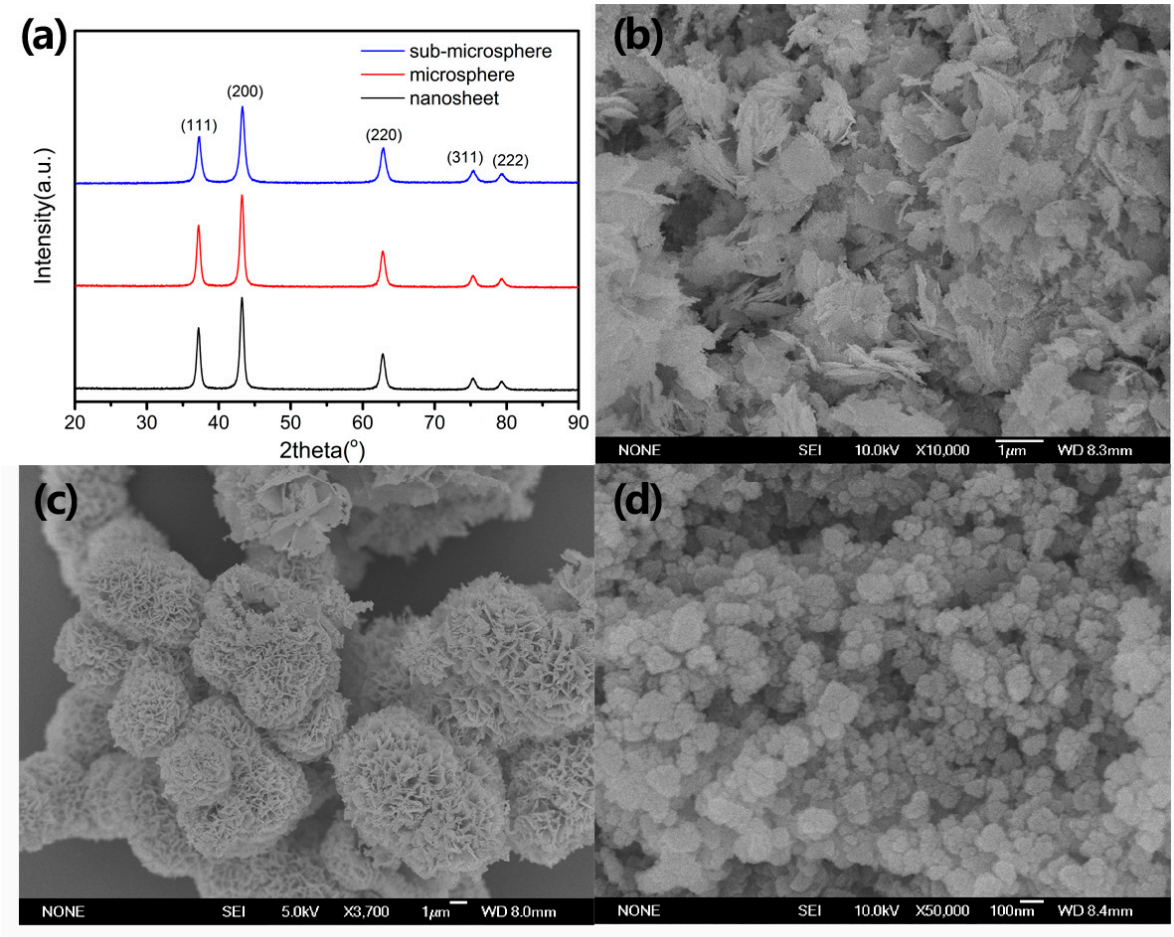

Figure 2. (**a**) XRD (Cu Kα, λ = 0.15406 nm) patterns and SEM images (secondary electron imaging mode) of as-prepared (**b**) nickel oxide (NiO) nanosheet; (**c**) NiO microsphere; and (**d**) NiO sub-microsphere.

In order to further study the morphology and microstructure of the NiO samples, TEM, high-resolution TEM (HRTEM), and selected area electron diffraction (SAED) patterns were performed and the results are shown in Figure 3. It can be seen from Figure 3a that the NiO nanosheet sample was composed of an aggregation of nanosheets, in accordance with the SEM observation (Figure 2b). The nanosheets are composed of many grains with diameters of 30–50 nm, and a large number of holes are also observed (Figure 3b). The SAED pattern exhibits a typical polycrystalline ring, which indicates that the material has good crystallinity (inset in Figure 3b). The HRTEM image (Figure 3c) demonstrates clear crystal lattice fringes with lattice spacing of 0.208 nm, corresponding to the (200) crystal plane of the NiO phase. Figure 3d indicates that the NiO microsphere sample was composed of about 2 μm microspheres and some fragmented aggregates with the size of 500 nm which could be caused by the ultrasonic vibration during the TEM sample preparation process. Figure 3e shows that the microsphere

consists of rod-like particles with a diameter of 20 nm and a length of 100 nm. The SAED pattern also indicates a typical polycrystalline ring (inset in Figure 3e). The clear lattice fringes observed in HRTEM images (Figure 3f) indicate the good crystallinity of the NiO microsphere sample. Figure 3g shows that there are many aggregations of sub-microspheres with a size of 100 nm in the NiO sub-microspheres. The high-magnification TEM image in Figure 3h indicates that the sub-microspheres are composed of many grains of 10–20 nm in size and a large number of well-distributed pores are observed. The SAED pattern is also a polycrystalline ring (inset in Figure 3h). The HRTEM image (Figure 3i) shows clear lattice fringes with a spacing of 0.244 nm, which can be attributed to the (111) crystal plane of the NiO phase. The corresponding energy dispersive spectroscopy (EDS) spectra (Figure S1) indicates that the atomic ratio of Ni and O in the samples are close to 1:1.

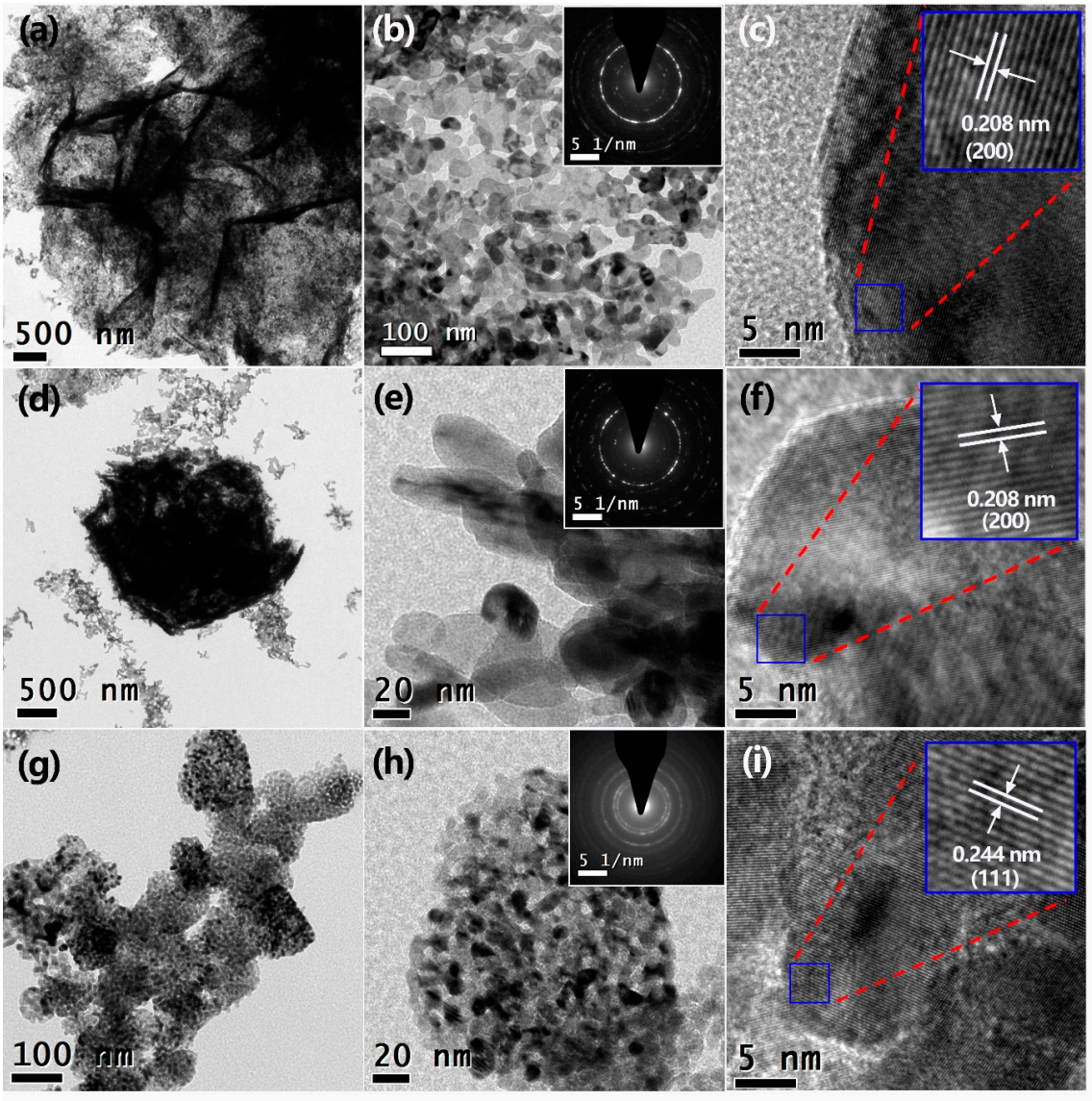

Figure 3. TEM and HRTEM images of as-prepared NiO nanostructures: (**a**) low-magnification TEM image, (**b**) high-magnification TEM image, and (**c**) HRTEM image of NiO nanosheet; (**d**) low-magnification TEM image, (**e**) high-magnification TEM image, and (**f**) HRTEM image of NiO microspheres; (**g**) low-magnification TEM image, (**h**) high-magnification TEM image, and (**i**) HRTEM image of NiO sub-microsphere. The insets in (**b**), (**e**), and (**h**) show the corresponding selected area electron diffraction (SAED) patterns.

To study the element composition and valence state of NiO sub-microsphere sample, XPS technique was performed (Figure 4). From the survey spectrum (Figure 4a), it can be seen that the binding energy peaks of Ni and O atoms exist in the spectrum. Figure 4b shows the Ni 2p binding energy spectrum. There are eight fitted binding energy peaks in the range of 850-885 ev. Among them, the two peaks located at 853.4 and 855.3 eV correspond to the characteristic peaks of Ni 2p 3/2, and the two peaks around 870.7 and 872.7 eV correspond to the Ni 2p 1/2 peak. The doublet peaks of 853.4 and 870.7 eV are related with Ni^{2+} component, and the peaks of 855.3 and 872.7 eV are ascribed to Ni^{3+} component [25]. The remaining four characteristic peaks at 860.6, 864.7, 877.9, and 880.9 eV are satellite peaks. Figure 4c shows the O1s binding energy spectrum. It can be fitted to three characteristic peaks of 529.2, 530.9, and 532.1 eV, which correspond to Ni-O bond, oxygen in OH^- groups, and adsorbed water on the surface of the sample, respectively. These results indicate the formation of NiO phase, which is consistent with XRD results.

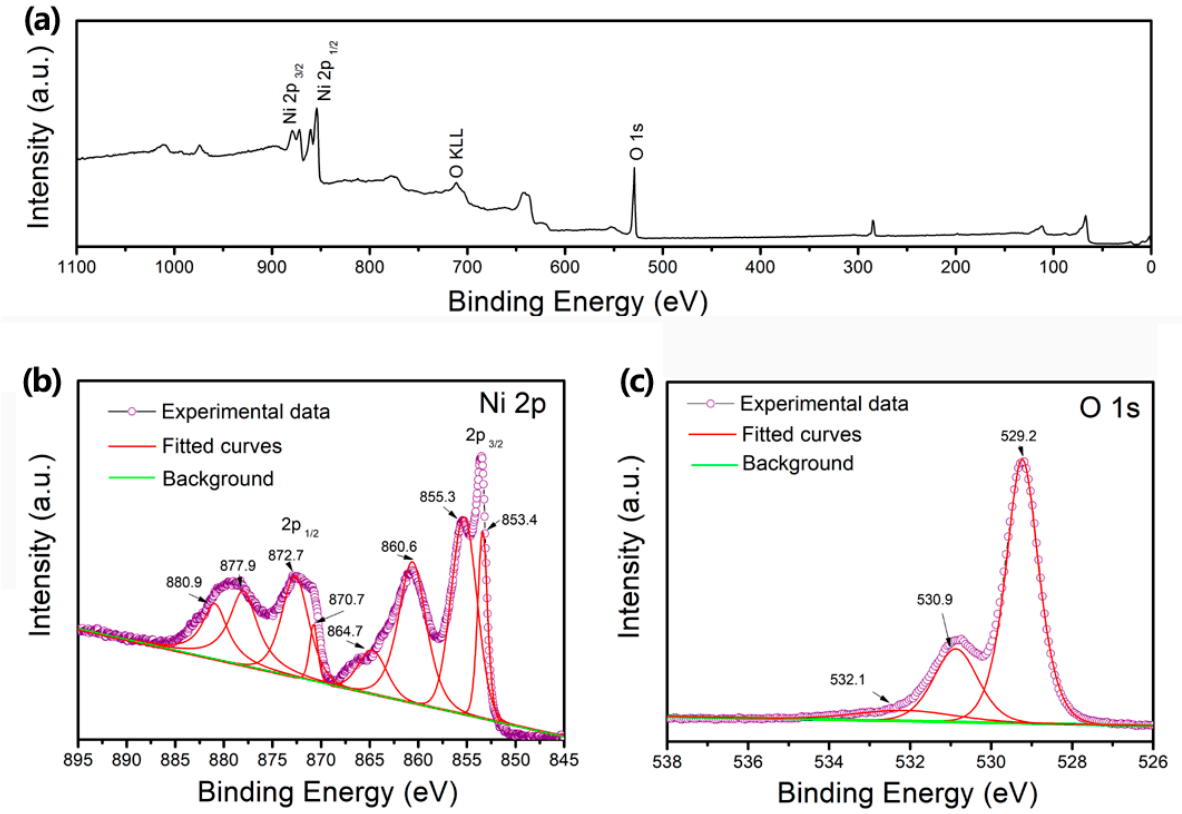

Figure 4. X-ray photoelectron spectroscopy (XPS) spectrum of as-prepared NiO sub-microsphere: (**a**) survey spectrum; (**b**) Ni 2p spectrum; and (**c**) O 1s spectrum.

Since porosities were observed in the NiO samples by TEM observation, the surface area and pore structure of the NiO samples were further investigated and the results are shown in Figure 5. The N_2 adsorption–desorption isotherm curve (Figure 5a) of the NiO nanosheet sample shows a typical IV type isotherm with a H2 hysteresis loop [26], which indicates the existence of a mesoporous structure in the sample. The BET surface area and pore volume are 40.5 m^2/g and 0.11 cm^3/g, respectively. The NiO microsphere sample exhibits a similar isotherm curve (Figure 5b), with the BET surface area of 19.8 m^2/g and pore volume of 0.06 cm^3/g. Figure 5c shows N_2 adsorption–desorption isotherm curve of the NiO sub-microsphere sample. It can be seen that the enclosure area increases obviously though the same IV type isotherm with a H2 hysteresis loop is observed. The BET surface area and pore volume are 89.5 m^2/g and 0.58 cm^3/g, respectively. Figure 5d shows the pore size distribution derived from the adsorption branches of the isotherm data in Figure 5a–c of the NiO samples. A peak centered at

about 3 nm was observed in the NiO nanosheet and microsphere samples. Comparatively, three peaks located at 9, 15, and 30 nm are observed in the NiO sub-microsphere sample, as well as the apparently increased peak intensity. From the above results, it can be concluded that the NiO sub-microspheres sample has the largest specific surface area and pore volume, which could be related to the smallest grain size of the NiO sub-microsphere sample, as observed in the TEM results (Figure 3).

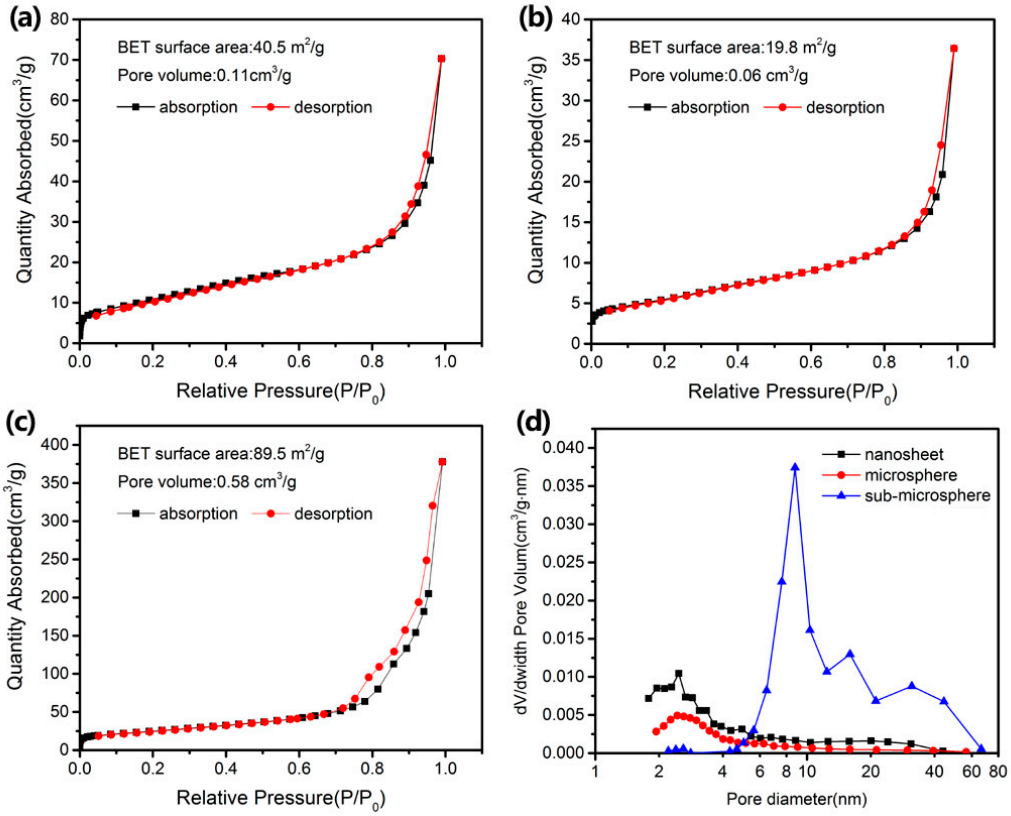

Figure 5. (**a**) N_2 adsorption–desorption isotherm curves of NiO nanosheet; (**b**) N_2 adsorption–desorption isotherm curves of NiO microsphere; (**c**) N_2 adsorption–desorption isotherm curves of NiO sub-microsphere; and (**d**) pore size distribution derived from the adsorption branches of the isotherm data of the as-prepared NiO nanostructures.

Combined with the above results, the synthesis route of mesoporous NiO hierarchical nanostructures can be summarized in Figure 6. By adjusting the ratio of Ni^{2+}/HMT, the precursor with multi-morphologies can be obtained. When the ratios of Ni^{2+}/HMT were 2:1 and 1:2, $Ni_3(NO_3)_2(OH)_4$ nanosheet and microsphere were obtained. Being calcined, they decomposed to the NiO phase and by-product gases such as NO_2, H_2O, and O_2 by the following reaction [26]:

$$Ni_3(NO_3)_2(OH)_4 \rightarrow 3NiO + 2NO_2(g) + 2H_2O(g) + \frac{1}{2}O_2(g) \quad (1)$$

When the ratio of Ni^{2+}/HMT was 1:3, $Ni(HCO_3)_2$ sub-microsphere was obtained, which decomposed to the NiO phase and gases of H_2O and CO_2 by the following reaction [27]:

$$Ni(HCO_3)_2 \rightarrow NiO + H_2O(g) + 2CO_2(g) \quad (2)$$

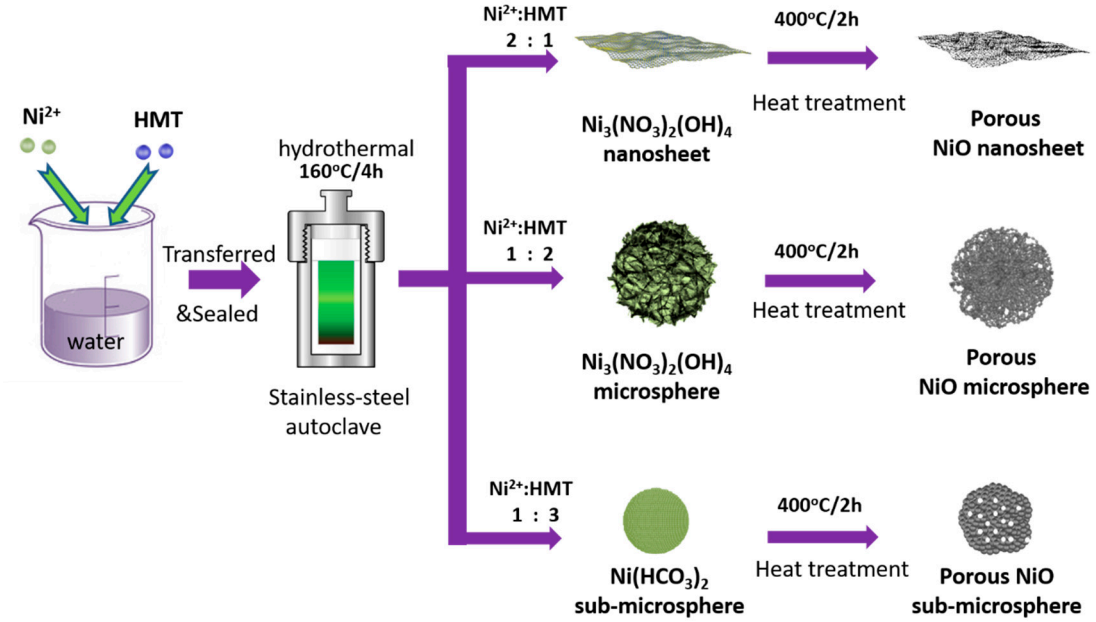

Figure 6. The synthesis route of hydrothermal reaction and subsequent calcination for mesoporous NiO hierarchical nanostructures.

The released by-product gases lead to the formation of a mesoporous structure in the NiO samples. To prove that the mesoporous structure was formed by calcination, the microstructure of an uncalcined microsphere precursor was studied by TEM, as shown in Figure S2. It clearly indicates the absence of mesoscale porosities in the uncalcined microsphere precursor. Thus, the calcination is helpful to the formation of the mesoporous structure.

3.2. *Catalytic Role of NiO Addtives*

Ammonium perchlorate (AP) is an important oxidant commonly used in rocket solid composite propellant. Its catalyzed thermal decomposition plays a key role in satellite launching and space exploration. The core part of catalyzed thermal decomposition of AP is the additives that can promote AP to achieve highly concentrated thermal decomposition at lower temperatures. The thermal decomposition of AP can be divided into two stages. One stage is usually in the range of 290–330 °C, which is called the low temperature decomposition (LTD) stage. The other stage occurs in the range of 350–450 °C and is called the high temperature decomposition (HTD) stage [28]. In the LTD stage, AP decomposes into NH_3 and $HClO_4$. The excess NH_3 continuously adsorbs on the AP surface to stop the LTD stage. When the temperature increases further, NH_3 adsorbed on the AP surface will desorb from the AP surface, and then the HTD of AP begins.

The catalytic role of as-prepared mesoporous NiO nanomaterials towards AP thermal decomposition was evaluated by the DTA technique. Figure 7a shows the DTA curves of pure AP and AP mixtures with NiO nanomaterials as additives. For pure AP, there is an endothermic peak at 248.8 °C and two exothermic peaks at 337.8 and 461.4 °C. Previous studies have shown that the endothermic peak at 248.8 °C corresponds to the transition temperature of AP from the rhombic phase to the cubic phase; the exothermic peak at 337.8 °C is associated with the LTD temperature (T_a) of AP, and the exothermic peak at 461.4 °C is ascribed to the HTD temperature (T_b) of AP. After adding NiO nanomaterials as additives, the DTA curve of the AP mixture has changed obviously. The phase transition temperature of AP did not change after adding NiO additives, which indicates that NiO additives have no effect on the phase transition temperature of AP [29]. Additionally, the intensity and area of the exothermic peak are obviously increased though the LTD temperatures of AP are slightly decreased. The HTD temperatures of AP are obviously decreased, and the exothermic peaks at a higher

temperature are weakened. It indicates that the NiO additives have an obvious catalytic role towards the thermal decomposition of AP.

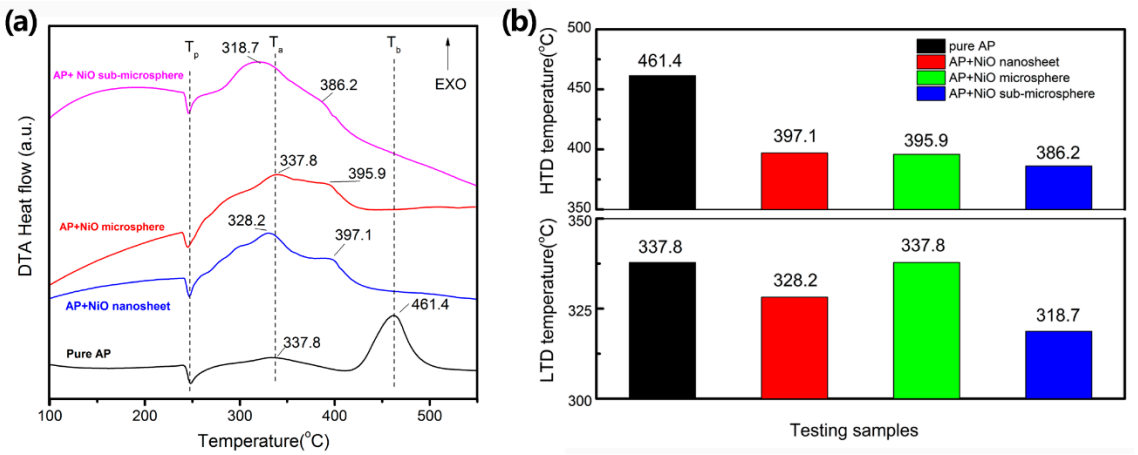

Figure 7. (**a**) Differential thermal analyzer (DTA) curves of pure ammonium perchlorate (AP) and AP mixture with as-prepared NiO additives; (**b**) histogram of high temperature decomposition (HTD) and low temperature decomposition (LTD) temperatures in (**a**).

In order to further study the catalytic effects, the LTD temperatures and HTD temperatures of different samples are compared, as shown in Figure 7b. It can be seen that NiO sub-microspheres exhibit the best catalytic role among all samples, which can reduce the HTD temperature of AP from 461.4 to 386.2 °C and the LTD temperate from 337.8 to 318.7 °C, respectively. It indicates that the HTD and LTD temperature of AP can be decreased by 75.2 and 19.1 °C. The catalytic activity of NiO sub-microsphere toward AP thermal decomposition is much better than the commercial spectrograde NiO reported by Wang et al. [29] with an HTD temperature of 412 °C. Although the mechanism of AP thermal decomposition is complex, we believe that the superior catalytic role of NiO sub-microsphere should be related to their large specific surface area, pore volume, and small grain size, which can facilitate gas diffusion and provide more reactive sites.

4. Conclusions

In this paper, mesoporous NiO hierarchical nanomaterials were prepared by a facile hydrothermal method and subsequent calcination. By adjusting the ratio of Ni^{2+}/HMT, the precursors of $Ni_3(NO_3)_2(OH)_4$ nanosheet, $Ni_3(NO_3)_2(OH)_4$ microsphere, and $Ni(HCO_3)_2$ sub-microsphere were prepared. After calcination at 400 °C for 2 h, the precursors can be transformed to mesoporous NiO nanosheet, microsphere, and sub-microsphere. When used as additives for AP thermal decomposition, the as-prepared NiO nanomaterials showed an obvious catalytic role. Among them, NiO sub-microspheres have the best catalytic role, which reduces the HTD and LTD temperature by 75.2 and 19.1 °C, respectively. Therefore, the synthetic route adopted in this paper can rapidly prepare mesoporous NiO hierarchical nanomaterials, which can be used as AP thermal decomposition additives.

Supplementary Materials: The following are available online at http://www.mdpi.com/2076-3417/9/13/2599/s1, Figure S1: EDS spectrum of (a) NiO nanosheet; (b) NiO sub-microsphere, Figure S2: (a) Low-magnification TEM image, (b) high-magnification TEM image; and (c) HRTEM image of the precursor of $Ni_3(NO_3)_2(OH)_4$ microsphere.

Author Contributions: S.Y. performed the experiments and wrote the paper; X.G. conceived and designed the experiments, analyzed the data, and revised the paper.

Funding: This work was funded by Natural Science Foundation of Fujian Province (2017J01676), the Key Research Foundation for Young Scholars of Fujian Education Department of China (JZ160486), and the Program for New Century Excellent Talents in Fujian Province University (Minjiaoke (2018) No. 47).

Conflicts of Interest: The authors declare no conflicts of interest.

References

1. Poizot, P.; Laruelle, S.; Grugeon, S.; Dupont, L.; Tarascon, J.M. Nano-sized transition-metal oxides as negative-electrode materials for lithium-ion batteries. *Nature* **2000**, *407*, 496–499. [CrossRef] [PubMed]
2. Macdonald, T.J.; Xu, J.; Elmas, S.; Mange, Y.J.; Skinner, W.M.; Xu, H.L.; Nann, T. NiO nanofibers as a candidate for a nanophotocathode. *Nanomaterials* **2014**, *4*, 256–266. [CrossRef] [PubMed]
3. Zhao, J.B.; Wu, L.L.; Zou, K. Fabrication of hollow mesoporous NiO hexagonal microspheres via hydrothermal process in ionic liquid. *Mater. Res. Bull.* **2011**, *46*, 2427–2432. [CrossRef]
4. Zhang, L.; Liu, P.F.; Li, Y.H.; Zu, M.Y.; Li, X.; Jiang, Z.; Wang, Y.; Zhao, H.; Yang, H.G. N-modified NiO surface for superior alkaline hydrogen evolution. *ChemSusChem* **2018**, *11*, 1020–1024. [CrossRef] [PubMed]
5. Wei, W.X.; Jiang, X.H.; Lu, L.D.; Yang, X.J.; Wang, X. Study on the catalytic effect of NiO nanoparticles on the thermal decomposition of TEGDN/NC propellant. *J. Hazard. Mater.* **2009**, *168*, 838–842. [CrossRef] [PubMed]
6. Luan, V.H.; Tien, H.N.; Hur, S.H.; Han, J.H.; Lee, W. Three-dimensional porous nitrogen-doped NiO nanostructures as highly sensitive NO_2 sensors. *Nanomaterial* **2017**, *7*, 313. [CrossRef] [PubMed]
7. Kumar, J.P.; Giri, S.D.; Sarkar, A. Mesoporous NiO with different morphology: Synthesis, characterization and their evaluation for oxygen evolution reaction. *Int. J. Hydrogen Energy* **2018**, *43*, 15639–15649. [CrossRef]
8. Yan, X.Y.; Tong, X.L.; Wang, J.; Gong, C.W.; Zhang, M.G.; Liang, L.P. Synthesis of mesoporous NiO nanoflake array and its enhanced electrochemical performance for supercapacitor application. *J. Alloy Compd.* **2014**, *593*, 184–189. [CrossRef]
9. Shenashen, M.A.; Kawada, S.; Selim, M.M.; Morsy, W.M.; Yamaguchi, H.; Alhamid, A.A.; Ohashi, N.; Lchinose, I.; El-Safty, S.A. Bushy sphere dendrites with husk-shaped branches axially spreading out from the core for photo-catalytic oxidation/remediation of toxins. *Nanoscale* **2017**, *9*, 7947–7959. [CrossRef]
10. Emran, M.Y.; Mekawy, M.; Akhtar, N.; Shenashen, M.A.; EL-Sewify, I.M.; Faheem, A.; El-Safty, S.A. Broccoli-shaped biosensor hierarchy for electrochemical screening of noradrenaline in living cells. *Biosens. Bioelectron.* **2018**, *100*, 122–131. [CrossRef]
11. Emran, M.Y.; Shenashen, M.A.; Abdelwahab, A.A.; Khalifa, H.; Mekawy, M.; Akhtar, N. Design of hierarchical electrocatalytic mediator for one step, selective screening of biomolecules in biological fluid samples. *J. Appl. Electrochem.* **2018**, *48*, 529–542. [CrossRef]
12. Emran, M.Y.; Shenashen, M.A.; Mekawy, M.; Azzam, A.M.; Akhtar, N.; Gomaa, H.; Selim, M.M.; Faheem, A.; El-Safty, S.A. Ultrasensitive in-vitro monitoring of monoamine neurotransmitters from dopaminergic cells. *Sens. Actuators B Chem.* **2018**, *259*, 114–124. [CrossRef]
13. Emran, M.Y.; Khalifa, H.; Gomaa, H.; Shenashen, M.A.; Akhtar, N.; Mekawy, M.; Faheem, A.; El-Safty, S.A. Hierarchical C-N doped NiO with dual-head echinop flowers for ultrasensitive monitoring of epinephrine in human blood serum. *Microchim. Acta* **2017**, *184*, 4553–4562. [CrossRef]
14. Akhtar, N.; Emran, M.Y.; Shenashen, M.A.; Khalifa, H.; Osaka, T.; Faheem, A.; Homma, T.; Kawarada, H.; El-Safty, S.A. Fabrication of photo-electrochemical biosensors for ultrasensitive screening of mono-bioactive molecules: The effect of geometrical structures and crystal surfaces. *J. Mater. Chem. B* **2017**, *5*, 7985–7996. [CrossRef]
15. Liu, W.Y.; Wu, J.; Yang, Y.; Yu, H.; Dong, X.T.; Wang, X.L.; Liu, Z.L.; Wang, T.T.; Zhao, B. Facile synthesis of three-dimensional hierarchical NiO microflowers for efficient room temperature H_2S gas sensor. *Nano J. Mater. Sci. Mater. Electron.* **2018**, *29*, 4624–4631. [CrossRef]
16. Zhou, Q.; Lu, Z.R.; Wei, Z.J.; Xu, L.N.; Gui, Y.G.; Chen, W.G. Hydrothermal synthesis of hierarchical ultrathin NiO nanoflakes for high-performance CH_4 sensing. *Front. Chem.* **2018**, *6*, 194. [CrossRef] [PubMed]
17. Ahirwar, D.; Bano, M.; Khan, I.; Sheikh, M.U.D.; Thomas, M.; Khan, F. Fabrication of hierarchically mesoporous NiO nanostructures and their role in heterogeneous photocatalysis and sensing activity. *J. Mater. Sci. Mater. Electron.* **2018**, *29*, 5768–5781. [CrossRef]
18. Zhang, H.; Chen, W.G.; Li, Y.Q.; Jin, L.F.; Cui, F.; Song, Z.H. 3D flower-like NiO hierarchical structures assembled with size-controllable 1D blocking units: Gas sensing performances towards acetylene. *Front. Chem.* **2018**, *6*, 472. [CrossRef] [PubMed]
19. Han, K.H.; Huang, H.; Gong, Q.H.; Si, T.T.; Zhang, Z.L.; Zhou, G.W. Temperature-induced hierarchical tremella-like and pinecone-like NiO microspheres for high-performance supercapacitor electrode materials. *J. Mater. Sci.* **2018**, *53*, 12477–12491. [CrossRef]

20. Cai, Y.; Ma, J.M.; Wang, T.H. Hydrothermal synthesis of α-$Ni(OH)_2$ and its conversion to NiO with electrochemical properties. *J. Alloy Compd.* **2014**, *582*, 328–333. [CrossRef]
21. Derbalah, A.; El-safty, S.A.; Shenashen, M.A.; Khairy, M. Hierarchical nanohexagon ceramic sheet layers as platform adsorbents for hydrophilic and hydrophobic insecticides from agricultural wastewater. *ChemPlusChem* **2015**, *80*, 1769–1778. [CrossRef]
22. Shi, M.J.; Cui, M.W.; Kang, L.T.; Li, T.T.; Yun, S.; Du, J.; Xu, S.D.; Liu, Y. Porous $Ni_3(NO_3)_2(OH)_4$ nano-sheets for supercapacitors: Facile synthesis and excellent rate performance at high mass loadings. *Appl. Surf. Sci.* **2018**, *427*, 678–686. [CrossRef]
23. Wang, H.F.; Wu, L.M.; Wang, Y.S.; Li, X.N.; Wang, Y.J. Facile synthesis of Ni nanoparticles from triangular $Ni(HCO_3)_2$ nanosheets as catalysts for hydrogen generation from hydrous hydrazine. *Catal. Commun.* **2017**, *100*, 33–37. [CrossRef]
24. Wang, X.S.; Chen, L.; Li, F.; Zhang, S.Q.; Chen, X.C.; Yin, J.J. Synthesis of hollow NiO nanostructures and their application for supercapacitor electrode. *Ionics* **2018**, *25*, 697–705. [CrossRef]
25. Hao, C.; Zhou, S.; Wang, J.J.; Wang, X.H.; Gao, H.W.; Ge, C.W. Preparation of hierarchical spinel $NiCo_2O_4$ nanowires for high-performance supercapacitors. *Ind. Eng. Chem. Res.* **2018**, *57*, 2517–2525. [CrossRef]
26. Sietsma, J.R.A.; Meeldijk, J.D.; Versluijs-Helder, M.; Broersma, A.; Dillen, A.J.V.; Jongh, P.E.D.; Jong, K.P.D. Ordered mesoporous silica to study the preparation of Ni/SiO_2 ex nitrate catalysts: Impregnation, drying, and thermal treatments. *Chem. Mater.* **2008**, *20*, 2921–2931. [CrossRef]
27. Li, Y.W.; Zheng, Y.Y.; Yao, J.H.; Xiao, J.R.; Yang, J.W.; Xiao, S.H. Facile synthesis of nanocrystalline-assembled nest-like NiO hollow microspheres with superior lithium storage performance. *RSC Adv.* **2017**, *7*, 31287–31297. [CrossRef]
28. Sharma, J.K.; Srivastava, P.; Singh, G.; Akhtar, M.S.; Ameen, S. Biosynthesized NiO nanoparticles: Potential catalyst for ammonium perchlorate and composite solid propellants. *Ceram. Inter.* **2015**, *41*, 1573–1578. [CrossRef]
29. Wang, Y.P.; Zhu, J.W.; Yang, X.J.; Lu, L.D.; Wang, X. Preparation of NiO nanoparticles and their catalytic activity in the thermal decomposition of ammonium perchlorate. *Thermochim. Acta* **2005**, *437*, 106–109. [CrossRef]